Environ Fluid Mech (2009) 9:207–235
DOI 10.1007/s10652-008-9091-6

ORIGINAL ARTICLE

Hierarchical modeling of the dilute transport of suspended sediment in open channels

Fabián A. Bombardelli · Sanjeev K. Jha

Received: 24 December 2007 / Accepted: 6 August 2008 / Published online: 11 September 2008

Abstract We propose, discuss and validate a theoretical and numerical framework for sediment-laden, open-channel flows which is based on the two-fluid-model (TFM) equations of motion. The framework models involve mass and momentum equations for both phases (sediment and water) including the interactive forces of drag, lift, virtual mass and turbulent dispersion. The developed framework is composed by the complete two-fluid model (CTFM), a partial two-fluid model (PTFM), and a standard sediment-transport model (SSTM). Within the umbrella of the Reynolds-Averaged Navier-Stokes (RANS) equations, we apply K–ε type closures (standard and extended) to account for the turbulence in the carrier phase (water). We present the results of numerical computations undertaken by integrating the differential equations over control volumes. We address several issues of the theoretical models, especially those related to coupling between the two phases, interaction forces, turbulence closure and turbulent diffusivities. We compare simulation results with various recent experimental datasets for mean flow variables of the carrier as well as, for the first time, mean flow of the disperse phase and turbulence statistics. We show that most models analyzed in this paper predict the velocity of the carrier phase and that of the disperse phase within 10% of error. We also show that the PTFM provides better predictions of the distribution of sediment in the wall-normal direction as opposed to the standard Rousean profile, and that the CTFM is by no means superior to the PTFM for dilute mixtures. We additionally report and discuss the values of the Schmidt number found to improve the agreement between predictions of the distribution of suspended sediment and the experimental data.

Keywords K–ε model · Partial two-fluid model · Reynolds-Averaged Navier-Stokes (RANS) equations · Sediment transport · Suspended sediments · Turbulence modeling · Two-fluid model (TFM) · Two-phase flows

F. A. Bombardelli (✉) · S. K. Jha
Department of Civil and Environmental Engineering, University of California, Davis, 2001 Eng. III, One Shields Ave., Davis, CA 95616, USA
e-mail: fabombardelli@ucdavis.edu

S. K. Jha
e-mail: skjha@ucdavis.edu

1 Introduction

Traditional approaches to quantify the dilute transport of sediments in open channels have consisted in representing the solid phase as a scalar field with concentration C [54,71]. In other words, the carrier fluid (water) has been usually considered as a quasi single-phase flow in those approaches, and the transport of sediments has been characterized via an advection-diffusion equation for C [37]. Further, the sediment phase has been customarily assumed to travel at the same stream-wise velocity of the *mixture* fluid [17,24,43,44,71] and its diffusivity in the wall-normal direction has been specified in terms of a balance between turbulent diffusion and the effect of gravity. These hypotheses, which lead to the well-known Rousean distribution of sediments under equilibrium conditions [58] do not work well in all cases. In fact, it has been reported repeatedly by various researchers that the profile of water velocity in open-channel flows deviates only slightly from the standard semi-logarithmic law [14,30,49,50; 51, p. 996] but, more importantly, that the distribution of the concentration of sediments in the wall-normal direction differs *appreciably* from that obtained through the *standard* Rousean equation [14, 28, p. 488; 50, p. 18, 51, p. 994].

Several attempts have been made to correct the above "standard" sediment-transport model. For instance, some authors have proposed to alter the semi-logarithmic law by modifying the value of the von-Kármán's constant [3,16,30,44,50; 51, p. 996]. In addition, some authors have suggested improving the advection-diffusion equation through the inclusion of a mechanism called "drift" [19], which would result from additional particle velocity fluctuations due to the uneven distribution of solid concentration in the flow. Another modification proposed by diverse researchers has consisted in simply adjusting the values of the Schmidt number (the ratio between the eddy viscosity of the flow and the diffusivity of suspended sediment) in the advection-diffusion equation, or in the *standard* Rousean equation to improve the agreement with data [14, 71, p. 81; 72].

From a multi-component flow perspective, Drew [22] employed the two-phase, turbulence-averaged mass and momentum equations for water and sediments to analyze sediment transport in open channels. Buoyancy and drag were considered to be the only interaction forces. Drew applied the mixing length theory to represent the Reynolds stresses. By using order-of-magnitude estimates, assuming a *dilute* mixture, and neglecting the relative velocity between the phases, Drew derived differential equations for the distributions of stream-wise velocity and suspended-sediment concentration in the wall-normal direction. Through numerical solutions of the equations, he compared model predictions with experimental data, and found that although the overall prediction of the model was good in terms of flow velocities, it could not accurately predict the near-bottom sediment concentrations. McTigue [47], in turn, combined the turbulence-averaged mass and momentum equations for solids and water in the stream-wise and wall-normal directions. Using scaling of the terms in the resulting momentum equation in the wall-normal direction, he recovered the classical balance between the downward flux of settling particles due to gravity and the diffusive flux due to turbulence. He applied three models for the diffusivity of the disperse phase, and compared the analytical predictions of the distribution of sediment concentration with experimental data. McTigue analyzed the behavior of the solution for the concentration in two layers characterized by different flow length scales. He concluded that different models show satisfactory predictions in both layers. Kobayashi and Seo [35] were perhaps the first in working with the complete two-fluid model (CTFM; see below) using six equations: two for the mass balance of each phase and four for the momentum balance of each phase in the wall-normal as well as the stream-wise directions. The interaction between fluid and sediment was represented through the forces of buoyancy and drag. Kobayashi and Seo investigated the regions of suspended-load

and bed-load separately. In the bed-load region, they considered the interaction of the solids and the bed. Kobayashi and Seo derived equations for the profiles of sediment concentration and for the relative velocity between water and sediment (which was ignored in previous contributions). The models were solved numerically and analytically, and predictions were compared with experimental data with partial success. Following Kobayashi and Seo [35], Cao et al. [11] also used a two-layered approach (suspension layer and bed layer). They employed mixture equations for the carrier phase and mass and momentum equations for the disperse phase. In their analysis, they emphasized that the selection of closure models for the turbulent diffusivity and eddy viscosity plays a critical role in the final result for the velocity and concentration profiles. They compared the analytically-predicted mean velocities and distribution of sediment concentration in the wall-normal direction with experimental data, obtaining satisfactory agreement. Villaret and Davies [73] presented a review of sediment transport models ranging from simplified approaches based on the passive scalar hypothesis to complex two-phase flow models. Drag and lift were considered as interaction forces in the two-fluid model. Villaret and Davies compared the performance of those models in predicting the mean velocity of the water and the distribution of the concentration of sediment. Based on their observations, they advocated the use of two-phase flow models to reduce the empiricism involved in the classical models.

Greimann et al. [28] included in their analysis a "drift velocity" in addition to the relative velocity between phases. They developed an analytical expression for the sediment concentration profile and the relative velocity in dilute flows from the complete two-fluid equations. They considered the following interaction forces between water and sediment: drag, added mass and lift. For turbulence closure, Greimann et al. employed the expressions of turbulence intensities developed by Nezu and Rodi [53] for clear water flows. Greimann et al. compared their analytical model with experimental datasets, obtaining satisfactory results. Greimann and Holly [29] extended the above model to non-dilute conditions by addressing the importance of particle–particle interactions, and the effect of particle inertia. Jiang et al. [33] also developed an analytical model for the distributions of sediment concentration and relative velocity. They combined the momentum equations for the carrier and the disperse phases and introduced simplifications to the resulting equation based on the assumption of dilute mixture and negligible particle inertia. Jiang et al. [33] applied the expressions of Nezu and Nakagawa [52] to represent the turbulence intensities and obtained a final equation for the distribution of sediment concentration similar to that of Greimann et al. [28]. Comparisons of results with experimental data showed more accurate predictions for the distribution of sediment concentration than those coming from the Rousean model and from the models of Greimann et al. [28] and Griemann and Holly [29]. Hsu et al. [31] obtained, in turn, the profile of sediment concentration in the wall-normal direction by using a semi-analytical approach and a numerical solution of the CTFM in combination with an extended K–ε turbulence closure. These authors were, to the best of our knowledge, the first to employ a turbulence treatment based on a two-equation model to address the fluctuations in the carrier fluid *in dilute sediment-transport studies* (see below the enumeration of contributions about sheet flows). In their comparison with experimental data, Hsu et al. [31] focused on the flow near the bed only, and found the predictions to be closer to the experimental data than the Rousean formula. They explained that the better prediction was due to the use of additional terms in the K–ε turbulence model; however, no comparison of turbulence statistics with data was presented.

Recent studies concerning sediment motion in very dense sheet flows have also used the CTFM equations (see for example [21,32,39,40]). Most of those authors have used K–ε type turbulence closures, but *no comparison of turbulence statistics with data has been presented*.

In addition to solid-water flows, there is a wealth of models for bubble-water flows, which use different levels of the TFM (see, for instance, [5] and [61]). Table 1 summarizes recent models for solid-water flows.

A detailed analysis of the above contributions reveals the following issues:

1. Different formulations have been adopted to address the dilute sediment-transport problem; however, no general guideline exists on the theory to use in any given case. For example, it is not clear whether the CTFM is needed for an accurate simulation of sediment transport in open channels, or whether the mixture equations are enough. While some authors have not considered other models than the CTFM and/or multi-group models in *bubbly* flows [67,75], other authors have shown that good predictions can be obtained with relatively simple models [5,60]. This discussion has not been pursued in sediment-transport problems.
2. The relative importance of the diverse forces in the TFM has not been determined for sediment-laden, open-channel flows yet. Related to this issue is the so-called "turbulent dispersion force" [23], which may be included in the momentum equation for both phases instead of the diffusive term in the mass balance equation (see [5]).
3. In the case of solid-water flows, different authors have compared model predictions with data in terms of mean-flow carrier velocities and the distribution of suspended-sediment concentration, but except in studies on oscillatory sheet flow [39] the velocity profile *of the disperse phase* has not been presented in papers on dilute sediment transport.
4. To the best of our knowledge no study has compared simulated turbulence statistics with data, considering the *sediment transport as a two-phase flow* [46]. This is relatively easy to understand in terms of the difficulties in measuring turbulence statistics in two-phase flows, some of which have been overcome only recently. As said, only Hsu et al. [31,32] have presented predicted turbulence statistics in dilute sediment-transport studies, but no comparisons with measurements have been reported. This is a crucial issue that provides strong motivation for the research presented herein.
5. Several terms have been added in some models to the equations of turbulent kinetic energy (K) and dissipation rate of turbulent kinetic energy (ε) in order to account for the role exerted by the disperse phase on the flow turbulence. However, these results need to be verified through additional systematic comparisons with recent datasets.

The main objective of this paper is then to introduce, discuss and validate a theoretical and numerical framework constituted by a set of models for the prediction of flow variables in *dilute* sediment-laden, open-channel flows. We address all points mentioned above and validate the framework with data in the range of fine sands. In Sects. 2 and 3, we present and analyze the theoretical models for general two-phase flows. The framework includes the 1D standard sediment transport model (1D SSTM) in addition to the 1D CTFM and the 1D PTFM. In Sect. 4, we detail the numerical treatment of the equations, and in Sect. 5 we describe the datasets selected for testing the models. Finally, in Sect. 6 we present the numerical results and the comparisons of model predictions with the datasets.

2 Theoretical and numerical models for two-phase flows

2.1 General equations for a complete two-fluid model (CTFM)

Based on the continuum assumption enforced for both phases, the TFM consists of mass, momentum and energy equations for each phase, which can be obtained by ensemble

Table 1 Two-phase models for solid-water flows

Reference data source	Complete TFM (Y/N)	Mixture equations for the carrier (Y/N)	Method (Num./Analyt.)	Interaction forces	Treatment of turbulence	Comparison with data on mean flow	Comparison with data on turbulent statistics (Y/N)
Drew [22]	N	Y	Num.	N/A	Mixing length	U_m, C	N
McTigue [47]	N	Y	Analyt.	N/A	Mixing length	C	N
Kobayashi and Seo [35]	Y	N	Analyt./ Num.	Drag	Corrected parabolic profile of the eddy viscosity	U_c, C	N
Cao et al. [11]	N	Y	Analyt.	N/A	Linear and parabolic distribution of eddy viscosity	U_m, C	N
Dong and Zhang [21]	Y	N	Num.	Drag, lift and virtual mass	Mixing length	U_c, U_d, C	N
Greimann et al. [28]	Y	N	Analyt.	Drag, lift and virtual mass	Parabolic distribution of eddy viscosity	C	N
Greimann and Holly [29]	Y	N	Analyt.	Drag and virtual mass	Parabolic distribution of eddy viscosity	C	N
Hsu et al. [31]	Y	N	Num.	Drag	K–ε Closure	U_c, C	N[a]
Hsu et al. [32]	Y	N	Num.	Drag, lift and virtual mass	K–ε Closure	U_c, C	N[a]
Longo [40]	Y	N	Num.	Drag, lift and virtual mass	K–ε Closure	U_c, C	N[a]
Liu and Sato [39]	Y	N	Num.	Drag, lift and virtual mass	Parabolic distribution of eddy viscosity	U_c, U_d, C	N

[a] Numerical results of turbulent quantities are presented

averaging the exact conservation equations for each phase [23]. In particular, the mass and momentum equations for the complete two-fluid model (CTFM) read, respectively

$$\frac{\partial\left(\alpha_k\left\langle\rho_k\right\rangle\right)}{\partial t}+\nabla\cdot\left(\alpha_k\left\langle\rho_k\right\rangle\left\langle\overrightarrow{U_k}\right\rangle\right)=\Gamma_k \tag{1}$$

$$\begin{aligned}&\frac{\partial\left(\alpha_k\left\langle\rho_k\right\rangle\left\langle\overrightarrow{U_k}\right\rangle\right)}{\partial t}+\nabla\cdot\left(\alpha_k\left\langle\rho_k\right\rangle\left\langle\overrightarrow{U_k}\right\rangle\otimes\left\langle\overrightarrow{U_k}\right\rangle\right)=-\alpha_k\nabla p_k\\&+\nabla\cdot\left[\alpha_k\left(\left\langle\underline{\underline{T_k}}\right\rangle+\underline{\underline{T_k^{\mathrm{Re}}}}\right)\right]+\alpha_k\left\langle\rho_k\right\rangle\left\langle\overrightarrow{b_k}\right\rangle+\overrightarrow{M_k}+\overrightarrow{U_{ki}}\,\Gamma_k\end{aligned} \tag{2}$$

In Eqs. 1 and 2, the subscript k indicates the phase, which could be the carrier (water with subscript c) or the suspended solids in the sediment-transport problem (with subscript d); α_k refers to the fraction of phase k; $<\cdot>$ indicates ensemble-averaged variables; ρ_k is the density, and $\overrightarrow{U_k}$ is the velocity vector of phase k; t refers to the time coordinate; Γ_k stands for mass sources (or sinks) due to convective or molecular fluxes at the interface of phase k; $\otimes$ implies the tensorial product; p_k denotes the pressure of phase k; and $\left\langle\underline{\underline{T_k}}\right\rangle$ and $\underline{\underline{T_k^{\mathrm{Re}}}}$ represent the ensemble-averaged and the remaining deviatoric stresses, respectively. In turn, $\vec{b}_k$ includes the group of volumetric forces such as gravity; $\vec{M}_k$ represents the interaction forces among phases; and $\overrightarrow{U_{ki}}$ refers to the velocity at the interface of phase k. The term $\overrightarrow{U_{ki}}\,\Gamma_k$ in Eq. 2 is usually disregarded. It has become customary to write [23, p. 226]:

$$\vec{M}_k=p_{ki}\nabla\alpha_k-T_{ki}\nabla\alpha_k+\vec{M}_k' \tag{3}$$

where the subscript i refers, again, to interface variables, and p_{ki} and T_{ki} denote the spherical and deviatoric parts of the stress tensor at the interface. The first two terms of Eq. 3 are usually neglected [23]. $\vec{M}_k'$ includes all the interactive forces, typically, due to drag, lift, virtual mass and turbulent dispersion.

2.2 Equations for a partial two-fluid model (PTFM)

The above equations are considered to be the "exact" equations for multi-phase flows; however, under some situations they lead to an ill-posed problem (see [23, p. 248]). In order to recover the structure of the Navier-Stokes equations, Buscaglia et al. [10] and Bombardelli [5] used the following definitions of mixture variables (with subscript m) in terms of ensemble-averaged magnitudes: $p_m=\langle p_c\rangle=\langle p_d\rangle$; $T_m=\alpha_c\langle T_c\rangle+\alpha_d\langle T_d\rangle$; $\rho_m=\alpha_c\langle\rho_c\rangle+\alpha_d\langle\rho_d\rangle$; $\rho_m U_m=\alpha_c\langle\rho_c\rangle\langle U_c\rangle+\alpha_d\langle\rho_d\rangle\langle U_d\rangle$. These equations are similar to a certain extent to those used by Cao et al. [11] and those discussed by Brennen [9].

Then, it is possible to: (a) Combine the mass and momentum equations for each phase given by (1) and (2); (b) use the above definitions; (c) invoke the dilute-mixture hypothesis and the Boussinesq approximation; and (d) *perform an average over turbulence*, in order to obtain the following mass and momentum equations for a dilute mixture (see [5,7,10]):

$$\nabla\cdot\left(\overrightarrow{U_m}\right)=0 \tag{4}$$

$$\frac{\partial\left(\rho_0\overrightarrow{U_m}\right)}{\partial t}+\nabla\cdot\left(\rho_0\overrightarrow{U_m}\otimes\overrightarrow{U_m}\right)+\nabla p_m=\nabla\cdot\left[\mu_{eff,m}\left(\nabla\overrightarrow{U_m}+\nabla\overrightarrow{U_m}^T\right)\right]+\rho_m\vec{g} \tag{5}$$

where the overbars for turbulence averaging have been dropped for simplicity; ρ_0 indicates a reference density; and the superscript T indicates the transpose tensor. Several authors (see [12,13,23]) have considered that the second average embedded in (4) and (5) is not required; however, we do believe it is necessary in order to obtain a diffusive term in the mass conservation equation of the disperse phase (see below). Moraga et al. [48] recently undertook an assessment of models for the dispersion due to turbulence in two-phase flows. They found that when the dominant forces are drag, buoyancy and turbulent dispersion both approaches (with single or double average) are equivalent. Bombardelli [5] provided a detailed discussion on the advantages of the double-averaging approach. In Eq. 5, $\mu_{eff,m}$ is the effective dynamic viscosity of the mixture in a Newtonian fluid, which is rigorously the sum of the turbulent (eddy) viscosity μ_T, and the laminar viscosity μ. (In our computations, we disregarded the latter as opposed to the former.) Further, in this paper we follow Buscaglia et al. [10], Bombardelli [5] and Bombardelli et al. [7] in considering *these mixture equations as a surrogate for the carrier fluid*.

For the disperse phase, we can average Eqs. 1 and 2 over turbulence, taking $k = d$, where d denotes the disperse phase, as before. This operation leads to the following equations (see [5,10]):

$$\frac{\partial\left(\alpha_d \rho_d\right)}{\partial t} + \nabla \cdot \left(\alpha_d \rho_d \overrightarrow{U_d}\right) = \nabla \cdot \left[\underline{\underline{D_d}} \cdot \nabla\left(\alpha_d \rho_d\right)\right] \tag{6}$$

$$\frac{\partial\left(\alpha_d \rho_d \overrightarrow{U_d}\right)}{\partial t} + \nabla \cdot \left(\alpha_d \rho_d \overrightarrow{U_d} \otimes \overrightarrow{U_d}\right) = -\alpha_d \nabla p_c + \nabla \cdot \left[\alpha_d \mu_{eff,d}\left(\nabla \overrightarrow{U_d} + \nabla \overrightarrow{U_d}^T\right)\right] + \alpha_d \rho_d \vec{g} + \overrightarrow{M_d} \tag{7}$$

where $\underline{\underline{D_d}}$ indicates the tensor of diffusion (or diffusivity tensor) and $\mu_{eff,d}$ the effective viscosity of the disperse phase, also equal to the sum of an eddy viscosity and the molecular viscosity. In these equations, we assumed the usual equivalence between the pressure of the disperse phase and the pressure of the continuous fluid, in addition to the Newtonian behavior for the stresses. The hypothesis of a Newtonian fluid adopted in this work is customary in dilute mixtures [23], where the effects of inter-particle collisions are relatively negligible (for a more detailed discussion, see [23, 56]). In a mixture-flow formulation, the diffusive term on the right-hand side of (6) provides the required transverse diffusion of the disperse phase.

Equations 4–7 constitute a modified set of equations to describe the two-fluid flow. We refer to this approach as a *partial two-fluid model* (PTFM). It becomes clear from these equations that only a one-way coupling between both phases is possible, because there is no interaction term (i.e., force) present in the governing equations for the carrier phase. On the other hand, it is well known that one-way coupling is an accurate representation of dilute mixtures [41].

It follows from Eq. 7 that a simplified version of the PTFM can be obtained by employing an algebraic model for $\vec{U}_d$ instead of using the full momentum equation:

$$\vec{U}_d = \vec{U}_m + \vec{W}_s \tag{8}$$

where $\vec{W}_s$ is the relative or "slip" velocity vector. This simplified approach was employed by Sokolichin and Eigenberger [60], Buscaglia et al. [10], Bombardelli [5] and Sokolichin et al. [61], in the context of bubble plumes; these authors obtained notable success in reproducing steady-state and unsteady experimental conditions (see [4]).

3 A 1D framework for dilute sediment-transport models in open channels

The framework is composed of a set of models and sub-models which include three levels of complexity: a 1D standard sediment-transport model (1D SSTM), a 1D PTFM, and a 1D CTFM, where the coordinate of analysis is the wall-normal direction (Fig. 1), for which $\frac{\partial}{\partial x} \approx 0$ and $\frac{\partial}{\partial y} \approx 0$. We assumed the slope of the channel, S, to be small and considered the disperse phase to be formed by sand particles of uniform size d_p.

3.1 1D standard sediment-transport model (1D SSTM)

The standard approach to model the sediment transport in open-channel flows considers the flow of the water–sediment *mixture*; therefore, it can be analyzed as a special case of Eqs. 4 and 5. Adopting the pair of axes of Fig. 1, we obtain the following mass, and two momentum equations in the x and z directions, respectively:

$$\text{Mass balance:} \frac{\partial W_m}{\partial z} = 0 \tag{9}$$

$$\text{Momentum balance in } x: \frac{\partial \left(\rho_0 U_m\right)}{\partial t} = \frac{\partial}{\partial z}\left[\nu_{eff,m} \frac{\partial \left(\rho_0 U_m\right)}{\partial z}\right] + \rho_m g S \tag{10}$$

$$\text{Momentum balance in } z\text{: } W_m = 0 \tag{11}$$

In the above equations, U_m and W_m denote the stream-wise and wall-normal components of $\overrightarrow{U_m}$; $\nu_{eff,m}$ is the effective kinematic viscosity of the mixture; and g is the acceleration due to gravity. In turn, the concentration of the sediment (C, volume of sediment/total volume) is computed from an advection-diffusion equation that follows from Eq. 6. Further, the simplified momentum equation given by (8) is used. Thus, the mass and the two momentum equations for the disperse phase (sediment) are:

$$\frac{\partial C}{\partial t} + W_d \frac{\partial C}{\partial z} = \frac{\partial}{\partial z}\left[D_d \frac{\partial C}{\partial z}\right] \tag{12}$$

$$U_d = U_m \tag{13}$$

$$W_d = -W_s \tag{14}$$

In the above equations, U_d and W_d denote the stream-wise and wall-normal components of $\vec{U}_d$; W_s is the settling (fall) velocity of the sediment, which can be calculated from relations such as that developed by Dietrich [20]; and D_d is the vertical diffusivity for sediment.

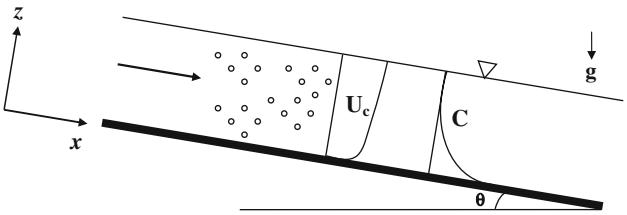

Fig. 1 Schematic of sediment-laden, open-channel flow

In this model, the fall velocity is considered constant throughout the entire depth. Instead of computing the diffusivity from the turbulence statistics [57], it is calculated in this standard model by using the Rousean distribution [54], as follows:

$$D_d = D_R = \kappa U_* \frac{z}{h}(h - z) \tag{15}$$

where κ is the von-Kármán constant; U_* is the wall-friction (shear) velocity; h is the water depth; z is the distance from the bottom of the channel in the wall-normal direction. (Turbulence modeling is employed as explained below for the eddy viscosity of the carrier fluid.) As it is clear from the governing Eqs. 9–14, the standard sediment-transport model is a decoupled one since it does not consider any interaction between sediments and water. This is the model currently used in many sediment-transport studies.

3.2 1D partial two-fluid model (1D PTFM)

As discussed earlier through Eqs. 4–8, the partial two-fluid model considers a mixture equation for the carrier phase and general two-fluid equations for the disperse phase. In this 1D PTFM, we also fixed W_d by using Eq. 8. For the interfacial forces, we considered drag, lift and virtual mass. In turn, the effect of the turbulent-dispersion force was represented through the diffusive term in the mass equation. Thus, the governing equations for mass and momentum in the stream-wise and wall-normal directions, for both phases, are as follows:

$$\frac{\partial W_m}{\partial z} = 0 \tag{16}$$

$$\frac{\partial (\rho_0 U_m)}{\partial t} = \frac{\partial}{\partial z}\left[\nu_{eff,m}\frac{\partial (\rho_0 U_m)}{\partial z}\right] + \rho_m g S \tag{17}$$

$$W_m = 0 \tag{18}$$

$$\frac{\partial (\alpha_d \rho_d)}{\partial t} + \frac{\partial (\alpha_d \rho_d W_d)}{\partial z} = \frac{\partial}{\partial z}\left[D_d \frac{\partial (\alpha_d \rho_d)}{\partial z}\right] \tag{19}$$

$$\frac{\partial (\alpha_d \rho_d U_d)}{\partial t} + \frac{\partial (\alpha_d \rho_d U_d W_d)}{\partial z} = \frac{\partial}{\partial z}\left[\nu_{eff,d}\frac{\partial (\alpha_d \rho_d U_d)}{\partial z}\right] + \alpha_d \rho_d g S + \chi_{d,D} F_{D,x} + \chi_{d,VM} F_{VM,x} + \chi_{d,L} F_{L,x} \tag{20}$$

$$W_d = -W_s \tag{21}$$

where the coefficients χ are used as indicators to include ($\chi = 1$) or exclude ($\chi = 0$) any interaction term; $\nu_{eff,d}$ is the effective kinematic viscosity of the disperse phase; the subscripts D, VM and L indicate drag, virtual mass and lift forces, respectively; and the subscript x indicates the stream-wise component of the forces. The interaction forces of drag, lift, and virtual mass are in turn expressed as follows, respectively (from the point of view of the disperse phase):

$$\overrightarrow{F_D} = \left[\frac{3}{4d_p}\alpha_d \rho_m C_D \sqrt{(U_m - U_d)^2 + (W_m - W_d)^2}\right] \times \left\{(U_m - U_d)\,\vec{i} + (W_m - W_d)\,\vec{k}\right\} \tag{22}$$

$$\overrightarrow{F_L} = C_L \alpha_d \rho_m \left\{-W_d \frac{\partial U_m}{\partial z}\vec{i} + (U_d - U_m)\frac{\partial U_m}{\partial z}\vec{k}\right\} \tag{23}$$

$$\overrightarrow{F_{VM}} = \frac{\alpha_d \rho_m}{2}\left\{\left[\frac{\partial (U_m - U_d)}{\partial t} - W_d \frac{\partial U_d}{\partial z}\right]\vec{i} - \left[\frac{\partial W_d}{\partial t} + W_d \frac{\partial W_d}{\partial z}\right]\vec{k}\right\} \tag{24}$$

where C_D is the drag coefficient; C_L is the lift coefficient; and $\vec{i}$ and $\vec{k}$ denote the unit vectors in the stream-wise and wall-normal directions, respectively.

Other forces are also included in some two-phase-flow models, such as the Faxen, Magnus and the Basset force. While the Faxen force is usually very small (it scales with $\left(d_p/l\right)^2$, where l is a flow length scale; [18,23]), the Basset force may be important in some cases (see [8]). However, since we are interested in the final steady state for the sediment particles, the Basset force is virtually zero. Magnus appears when there is particle rotation, and we are not considering particle rotation here.

3.3 1D complete two-fluid model (1D CTFM)

The governing equations of the 1D CTFM can be derived from the general equations presented in Sect. 2.1:

$$\frac{\partial W_c}{\partial z} = 0 \tag{25}$$

$$\frac{\partial \left[(1-\alpha_d)\,\rho_c U_c\right]}{\partial t} = \frac{\partial}{\partial z}\left\{\nu_{eff,c}\frac{\partial \left[(1-\alpha_d)\,\rho_c U_c\right]}{\partial z}\right\} + (1-\alpha_d)\,\rho_c\, g\, S - \chi_{c,D} F_{D,x} - \chi_{c,VM} F_{VM,x} - \chi_{c,L} F_{L,x} \tag{26}$$

$$W_c = 0 \tag{27}$$

$$\frac{\partial (\alpha_d \rho_d)}{\partial t} + \frac{\partial (\alpha_d \rho_d W_d)}{\partial z} = \frac{\partial}{\partial z}\left[D_d \frac{\partial (\alpha_d \rho_d)}{\partial z}\right] \tag{28}$$

$$\frac{\partial (\alpha_d \rho_d U_d)}{\partial t} + \frac{\partial (\alpha_d \rho_d U_d W_d)}{\partial z} = \frac{\partial}{\partial z}\left[\nu_{eff,d}\frac{\partial (\alpha_d \rho_d U_d)}{\partial z}\right] + \alpha_d \rho_d\, g\, S + \chi_{d,D} F_{D,x} + \chi_{d,VM} F_{VM,x} + \chi_{d,L} F_{L,x} \tag{29}$$

$$\frac{\partial (\alpha_d \rho_d W_d)}{\partial t} + \frac{\partial (\alpha_d \rho_d W_d W_d)}{\partial z} = -\alpha_d \frac{\partial P_c}{\partial z} + \frac{\partial}{\partial z}\left[\nu_{eff,d}\frac{\partial (\alpha_d \rho_d W_d)}{\partial z}\right] - \alpha_d \rho_d\, g \cos\theta + \chi_{d,D} F_{D,z} + \chi_{d,VM} F_{VM,z} + \chi_{d,L} F_{L,z} \tag{30}$$

It is worth noticing that the presence of interactive forces in Eq. 26 includes the possibility of two-way coupling. In the 1D CTFM, the motion of sediment in the vertical direction is expressed through Eq. 30 instead of using a value obtained from an algebraic relation (cf. Eq. 21). The subscript m in the Eqs. 22–24 for the forces is changed for that of the carrier in the CTFM. A hydrostatic pressure distribution was assumed in Eq. 30.

3.4 Turbulence closure

The turbulent eddy viscosity for the carrier phase, μ_T, and the diffusivity of sediment, D_d, are usually formulated in terms of the turbulent kinetic energy (TKE) and the dissipation rate of turbulent kinetic energy (DTKE) as follows:

$$\mu_T = \rho \nu_T = \rho C_\mu \frac{K^2}{\varepsilon} \tag{31}$$

$$D_d = C_\mu \frac{K^2}{\varepsilon} \frac{1}{\sigma} \tag{32}$$

where σ is the Schmidt number (defined in the Sect. 1), and $C_\mu = 0.09$.

In most works found in the literature, no treatment for the disperse phase turbulence has been provided. Implicitly, this is equivalent to assuming that the turbulence in the disperse phase is in equilibrium with the continuous phase turbulence. In single-phase flows, K and ε are obtained by solving standard equations which are mostly models on their own [38,57]. *There are no such widely accepted transport equations for* K and ε for two-phase flows. From the derivations of these transport equations for single-phase flows, it can be expected that the interaction forces present in the momentum equation of the carrier phase introduce additional terms in the final equations. Elghobashi and Abou-Arab [25] and Kataoka and Serizawa [34] presented the most general forms of the K–ε model for two-phase flows. They considered only the drag force in their momentum equation, however. Herein, we employed an extended version of the K–ε model similar to that of Hsu et al. [31]. Some authors have also used volume fractions of the carrier phase multiplying terms in the equations for the TKE and the DTKE. We believe that this is not required, given the dilute-mixture nature of the flows analyzed in this paper. We thus used the transport equations for TKE and DTKE in the following form:

$$\frac{\partial (\rho_c K)}{\partial t} = \frac{\partial}{\partial z}\left[\frac{\nu_T}{\sigma_K}\frac{\partial (\rho_c K)}{\partial z}\right] + P_S - \rho_c \varepsilon + S_K \tag{33}$$

$$\frac{\partial (\rho_c \varepsilon)}{\partial t} = \frac{\partial}{\partial z}\left[\frac{\nu_T}{\sigma_\varepsilon}\frac{\partial (\rho_c \varepsilon)}{\partial z}\right] + C_{\varepsilon 1} P_S \frac{\varepsilon}{K} - C_{\varepsilon 2}\rho_c \frac{\varepsilon^2}{K} + S_\varepsilon \tag{34}$$

where $P_S = \mu_T \left(\frac{\partial U_c}{\partial z}\right)^2$ is the shear production of turbulence; and S_K and S_ε are the additional terms in the equations. (When we use the PTFM, the subscript c above is changed to m.) Hsu et al. proposed the following expressions for these additional terms:

$$S_K = S_{K1} + S_{K2}; \quad S_\varepsilon = 1.2\, S_K \frac{\varepsilon}{K}; \tag{35}$$

with:

$$S_{K1} = -\frac{2\rho_d \alpha_d K}{T_P + T_L}, \text{ and}$$

$$S_{K2} = \frac{3}{4 d_p}\rho_c C_D \sqrt{(U_c - U_d)^2 + (W_c - W_d)^2}\quad \nu_T \frac{\partial \alpha_d}{\partial z}(W_c - W_d) \tag{36}$$

In the above equations, S_{K1} represents the correlation between the fluid and sediment velocity fluctuations, and S_{K2} represents the production of TKE due to the drag force [31,36]. In turn, the scales T_P (particle time scale) and T_L (flow time scale) are given by:

$$T_P = \frac{\rho_d}{\frac{3}{4 d_p}\rho_c C_D \sqrt{(U_c - U_d)^2 + (W_c - W_d)^2}}; \quad T_L = 0.165 \frac{K}{\varepsilon} \tag{37}$$

We modified this particle time scale from Hsu et al.'s expression for a non-linear drag force.

3.5 Other closures to the models

The drag coefficient was computed as follows [18]:

$$C_D = \frac{24}{\mathrm{Re}_r}\left(1 + 0.15\,\mathrm{Re}_r^{0.687}\right) \tag{38}$$

where $\mathrm{Re}_r = \frac{\rho_c |U_c - U_d| d_p}{\mu}$ is the explicit particle Reynolds number [54].

Several authors have proposed different formulas to determine the Schmidt number. We recall herein that the Schmidt number is the ratio between the eddy viscosity of the flow and the diffusivity of suspended sediment. Van Rijn [72] suggested a uniform Schmidt number throughout the depth, to be computed from:

$$\frac{1}{\sigma} = 1 + 2\left[\frac{W_s}{U_*}\right]^2 \quad \text{for } 0.1 < \frac{W_s}{U_*} < 1 \tag{39}$$

This equation gives an always less-than-one value of the Schmidt number. Instead of using a uniform value of the Schmidt number throughout the depth of the channel, Amoudry et al. [1] proposed a concentration-dependent Schmidt number, as follows:

$$\sigma = \sigma_o\left[1 - \frac{C}{C_o}\right] + \left[\frac{C}{C_o}\right]^q \tag{40}$$

where σ_o and q are empirical constants; C is the local concentration of sediment and C_o is the reference sediment concentration. Czernuszenko [19] suggested the following diffusion coefficient: $D_d = \nu_{T,c} + \varepsilon_{drift}$, where $\varepsilon_{drift} = \frac{\pi}{2} d_p \sqrt{\overline{U_d'^2}}$, $\sqrt{\overline{U_d'^2}}$ indicates the rms of the stream-wise fluctuations of the disperse phase and the overbar refers to the time average. (This $\sqrt{\overline{U_d'^2}}$ of the disperse phase is taken to be equal to $\sqrt{\overline{U_c'^2}}$ of the carrier.) Combining Czernuszenko's expression with the definition of σ, we obtain

$$\sigma = \frac{1}{1 + \frac{\varepsilon_{drift}}{\nu_{T,c}}} \tag{41}$$

In the comparison with data of Sect. 6, we obtain the value of the Schmidt number that best fits the experimental datasets, and also test Eq. 41.

The stress terms on the momentum equations for the disperse phase result from intergranular stresses (small in a dilute flow) and stress developed from the interaction between the carrier and the sediment. In most studies of bubbly flows, this term has been neglected on grounds of the small ratio of ρ_d/ρ_c [59,68]. Some studies on two-phase jets have used a relation between $\nu_{T,c}$ and $\nu_{T,d}$ proposed by Chen and Wood [15]:

$$\nu_{T,c} = \nu_{T,d}\,(1 + St) \tag{42}$$

where $St = t_*/T_L$ is the Stokes number; and $t_* = \frac{\rho_d d_p^2}{18\mu}$ is the Stokes particle adaptation time [18].

3.6 Boundary conditions

We evaluated the shear stress at the wall by computing the velocity in the first control volume via the semi-logarithmic velocity law [26]. We also enforced a zero Neumann condition

at the upper boundary for fluid and sediment horizontal velocities. The well-known wall functions were used as boundary condition for K and ε at the bottom, whereas the no-flux condition was imposed for ε at the top boundary. It is apparent that the motion of sediment will produce additional stresses close to the bed and hence the boundary conditions need to be modified in the case of two-phase flow as opposed to their single-phase counterparts. In the case of turbulent *bubbly* flows, Troshko and Hassan [68,69] reported an improvement in their predictions by using a modified law of the wall. We tested their proposals in this paper, too.

We imposed a Neumann condition for the sediment at the bottom. While simulating the test case of Muste et al. [50], the sediment fraction at the bottom ($\alpha_{d,b}$) was adopted to be the largest measured value close to the bed (at $z/h = 0.009$). In the case of Lyn [43], the value of the sediment fraction (sediment concentration) close to the bed was not available, and the data were extrapolated in order to obtain the value at the wall [54]. At the free surface, a null flux of sediment needs to be imposed. To that end, we adopted a Dirichlet boundary condition for the sediment concentration, $C = 0$, and a null diffusivity at the top. The null sediment concentration guarantees a zero advective flux at the top, while the zero diffusivity eliminates the diffusive contribution to the flux therein. The zero diffusivity is automatically obtained with the Rousean profile in the SSTM, but it needs to be enforced with a null eddy viscosity for the carrier through a zero TKE at the boundary (i. e., since $D_d = \nu_T/\sigma$, $D_d = 0$ when $\nu_T = 0$). Summarizing, the boundary conditions applied in the present analysis were:

$$D_d \frac{\partial C}{\partial z}\bigg|_{z=0} = -C_b W_s; \quad D_d \frac{\partial \alpha_d}{\partial z}\bigg|_{z=0} = -\alpha_{d,b} W_s \tag{43}$$

$$K|_{z=0} = \frac{U_*^2}{(c_\mu)^{1/2}}; \quad \varepsilon|_{z=0} = (c_\mu)^{3/4} \frac{K^{3/2}}{\kappa d_1} \tag{44}$$

where d_1 is the distance from the boundary to the center of the near-boundary grid cell [26].

$$\text{Top boundary: } \frac{\partial U_c}{\partial z} = \frac{\partial U_d}{\partial z} = \frac{\partial U_m}{\partial z} = \frac{\partial W_d}{\partial z} = W_c = W_m = 0 \tag{45}$$

$$\left(C W_s + D_R \frac{\partial C}{\partial z}\right)\bigg|_{z=h} = \left(C W_s + D_d \frac{\partial \alpha_d}{\partial z}\right)\bigg|_{z=h} = 0 \tag{46}$$

$$K|_{z=h} = \frac{\partial \varepsilon}{\partial z}\bigg|_{z=h} = 0 \tag{47}$$

4 Numerical implementation

The theoretical models presented in previous sections were solved numerically by extending a 1D flow solver, originally intended for single-phase flows [63]. This solver has been applied to a wide range of studies related to boundary layers in lakes, oceans and the atmosphere [2,64]. It has embedded the following general equation implemented:

$$\frac{\partial \Phi}{\partial t} = \frac{\partial}{\partial z}\left[\Gamma_\Phi \frac{\partial \Phi}{\partial z}\right] + S_\Phi \tag{48a}$$

where Φ indicates the dependent variable to be solved at a time; Γ_Φ is the exchange coefficient; and S_Φ is the source/sink term. The general differential equation is integrated over a control volume which leads to the following algebraic form [63]:

$$D\,(i)\,\Phi\,(i) = A(i)\Phi\,(i+1) + B\,(i)\,\Phi\,(i-1) + C\,(i) \tag{48b}$$

where $A(i)$, $B\,(i)$, $C\,(i)$, and $D\,(i)$ are matrix coefficients, which are defined as follows: $A(i) = T_+/Ar(i)$; $B(i) = T_-/Ar(i)$; $C(i) = \Phi_U(i)\Delta z(i)/\Delta t + \Delta z(i)S(i)$; and $D(i) = \Delta z(i)/\Delta t + (T_+ + T_-)/Ar(i) - \Delta z(i)S'(i)$. In the above definitions, i indicates the index of the control volume, which starts with a value of 1 at the very bottom; Ar and Δz are the corresponding area and height of the control volume, respectively; Δt is the time interval of the computation; Φ_U is the value of the dependent variable coming from the previous time step; S and S' are the components of the source term S_Φ (see Eq. 48a); and T_+ and T_- result from the integration of the diffusion term of Eq. 48a over the control volume. A more detailed description of the discretization can be found in Svensson [63], Svensson et al. [65] and Patankar [55]. Equation 48b has a tri-diagonal matrix form which can be solved by the Thomas algorithm.

The convective term in the equations of the different models was treated as a source/sink term via an upwinding scheme in an explicit manner. The finite difference form of the convective term thus becomes [26]:

$$-\frac{\partial\,(W_d\Phi)}{\partial z} = -\frac{\left(W^t_{d,i+1}\Phi^t_{i+1} - W^t_{d,i}\Phi^t_i\right)}{\Delta z} \tag{49}$$

where i increases upwards and W_d is directed downwards. The interaction forces of drag, lift and virtual mass, and additional terms in the K, and the ε equations were treated as extra source terms and set up in the model using the same approach as explained in Eq. 49.

5 Experimental datasets selected to test the models

The observation of two-phase flows is intrinsically difficult. In sediment-transport measurements, only recently it has been possible to differentiate between the motion of the carrier from that of the disperse phase [49]. Thus, most experimental datasets available in the literature present velocity profiles for the mixture flow only. Table 2 summarizes the main available datasets for sediment-laden, open-channel flows. It is possible to see that in most cases the particle sizes ranged from 100 to 300 microns. In Table 3, we detail the variables observed in the tests selected for our analysis: Lyn [43], Muste and Patel [49], and Muste et al. [50]. In Table 4, we describe the features of the flumes, and the characteristics of the sediment particles employed in the tests.

Lyn [43–45] carried out 15 experiments in a flume with a bed both in equilibrium and in starved conditions, to observe the effect of sediments on flow resistance and turbulence statistics. In his study, the size of natural sand ranged from 0.15 to 0.24 mm. We selected the

Table 2 List of datasets on sediment-laden, open-channel flows

Reference data source	Particle diameter (mm)
Muste et al. [50]	0.21–0.25
Muste and Patel [49]	0.21–0.25
Wang and Qian [74]	0.137
Coleman [17]	0.105–0.42
Taggart et al. [66]	0.15–0.28
Einstein and Chien [24]	0.396
Vanoni [70]	0.103–0.134
Lyn [43]	0.15–0.24

Table 3 List of datasets used in this study

Reference data source	Instruments employed for velocity measurements	Variables observed[a]
Lyn [43]	Laser-Doppler anemometry	V_{mix}, C
Muste and Patel [49]	Discriminator laser-Doppler velocimetry	V_c, V_d, T
Muste et al. [50]	Particle image velocimetry and Particle tracking velocimetry	V_c, V_d, C, T

[a] V: velocity profiles; mix: mixture; c: carrier phase; d: disperse phase; C: concentration profile; T: turbulence statistics

Table 4 Summary of flow characteristics in the experiments selected

Reference data source	Case	Depth (cm)	Slope	Particle diameter (mm)	Settling (fall) velocity (m/s)	Shear velocity (m/s)	Re_p
Lyn [43]	1965EQ	6.5	0.00251	0.19	0.023	0.0375	10.54
Muste and Patel [49]	SL01	12.9	0.000739	0.25	0.024	0.0324	15.90
Muste et al. [50]	NS1	2.1	0.0113	0.25	0.024	0.042	15.90

Note: The settling velocities in these tests were obtained from formulas; they were not measured

test 1965EQ for comparison with our numerical results, where EQ refers to equilibrium bed conditions. Lyn [43] considered only the mixture flow in his analysis and, hence, the velocity of the disperse phase is not available.

We also selected the tests SLO1 of Muste and Patel [49], and NS1 of Muste et al. [50]. Muste and Patel [49] presented three series of experiments with various concentrations of sediment in the flow. In test SLO1, the profiles of the water velocity, particle velocity, and turbulence statistics were obtained. However, Muste and Patel [49] did not provide information about the distribution of sediment concentration. In Muste et al.'s tests natural sand (NS) and neutrally buoyant sediment (crushed nylon) were used. Muste et al. [50] provided profiles of mean-flow variables, *as well as turbulence statistics*. We selected the case NS1, because it has the lowest volumetric concentration.

In the works mentioned above, the roughness of the bed of the channel was not provided. Lyn [44] stated that the flume was not perfectly smooth and that it was covered with a layer of sand; Muste and Patel [49] mentioned that the channel bed was made up of concrete. In the case of Muste et al. [50], the channel bed was formed of smooth stainless steel. We have obtained the bed roughness in each case by fitting the semi-logarithmic law to the experimental data of the water/mixture velocity. According to well-known criteria for assessing the wall behavior, we determined that it was close to being smooth in all three cases.

6 Numerical results

6.1 Grid independence tests

Initially, we carried out tests to determine that our numerical results were indeed grid independent. To that end, we observed the response of computed solutions to diverse values of the spatial and time steps. Given the adopted ensemble- and Reynolds-averaged approaches and given the particle sizes of the selected tests, the number of cells in our computations should

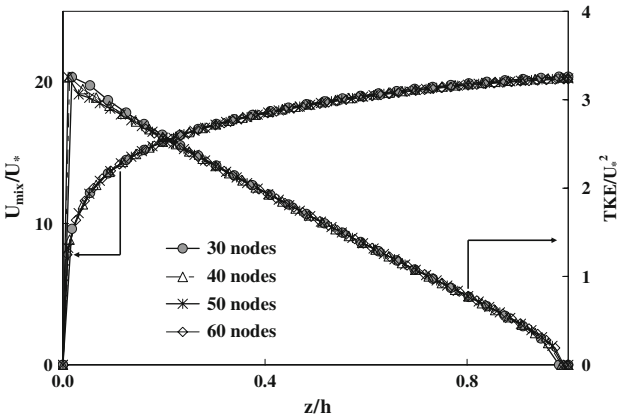

Fig. 2 Comparison of simulated values of the mixture stream-wise velocity component and the distribution of the TKE obtained using different meshes. Experimental tests of Muste et al. [50]

be of the order of a few tens. Based on this, we obtained solutions with meshes consisting of 30–60 cells. The time step was determined through a pseudo-Courant number, developed herein in terms of the fall velocity: $\Delta z/\Delta t > W_s$. We varied the time step from 0.001 to 0.1 s, adopting the value of the fall velocity for each test. The simulations were performed for a long time (of the order of 10,000 s of simulation time). We found that the computed profiles of velocity and sediment concentration reached a steady state after about 1,000 s. We tested the grid independence for the different experimental cases selected, with diverse sediment mean diameters. Profiles of the mixture and TKE are shown in Fig. 2 for different meshes pertaining to the case of Muste et al. It is possible to see that 50 or 60 cells can provide indistinguishable solutions. Similar results were obtained for all tests.

6.2 Description of the runs with different model variants

Table 5 summarizes the set of runs undertaken to observe the effect of different model formulations on the prediction of flow variables, and to assess their ability to interpret diverse experimental datasets. In Run 1, we employed the 1D SSTM and compared the numerical results with the well-known semi-logarithmic law for the mixture, and with the Rousean profile of sediment concentration (recall that the results of the turbulence closure are not used to compute the sediment diffusion coefficient in this run).

In Runs 2 and 3, the 1D PTFM and 1D CTFM were employed to test the influence of the complexity of the model on the results. One advantage of the 1D CTFM over the 1D PTFM is that the velocity of the disperse phase in the wall-normal direction is computed. We included only the drag force in the stream-wise direction in the 1D PTFM; buoyancy is *implicitly* included in the fall velocity in the 1D PTFM and it is *explicitly* included in the 1D CTFM. Tests 2 and 3 also reflect coupling, since the 1D PTFM implies essentially one-way coupling.

In Runs 4 and 5, we tested the importance of the forces of lift and virtual mass in addition to drag and buoyancy. Then, we assessed the relevance of the S_K and S_ε terms (Eqs. 33 and 34) in the K–ε turbulence closure with Runs 6 and 7. In Runs 2–7, we adopted a Schmidt number equal to 1 and selected an eddy viscosity of the disperse phase equal to the eddy viscosity of the carrier. In Runs 8 and 9, we investigated two cases for the eddy viscosity

Table 5 List of runs developed in this work

Run	Model	Interaction force	Diffusion coefficient of sediment	Eddy viscosity of the disperse phase	Turbulence closure Standard/ extended
1	1D SSTM	N/A	$D_d = D_R$	N/A	Standard
2	1D PTFM	Drag+Buoy.	$D_d = \nu_{T,m}$	$\nu_{T,d} = \nu_{T,m}$	Standard
3	1D CTFM	Drag+Buoy.	$D_d = \nu_{T,c}$	$\nu_{T,d} = \nu_{T,c}$	Standard
4	1D PTFM	Drag and Lift+Buoy.	$D_d = \nu_{T,m}$	$\nu_{T,d} = \nu_{T,m}$	Standard
5	1D PTFM	Drag, Lift and Virtual mass+Buoy.	$D_d = \nu_{T,m}$	$\nu_{T,d} = \nu_{T,m}$	Standard
6	1D PTFM	Drag+Buoy.	$D_d = \nu_{T,m}$	$\nu_{T,d} = \nu_{T,m}$	Extended
7	1D CTFM	Drag+Buoy.	$D_d = \nu_{T,c}$	$\nu_{T,d} = \nu_{T,c}$	Extended
8	1D PTFM	Drag+Buoy.	$D_d = \nu_{T,m}$	$\nu_{T,d} = 0$	Standard
9	1D PTFM	Drag+Buoy.	$D_d = \nu_{T,m}$	$\nu_{T,m} = \nu_{T,d}\,(1 + St)$	Standard
10	1D PTFM	Drag+Buoy.	$D_d = D_R$	$\nu_{T,d} = \nu_{T,m}$	Standard
11	1D PTFM	Drag+Buoy.	$D_d = \nu_{T,m} + \varepsilon_{drift}$	$\nu_{T,d} = \nu_{T,m}$	Standard
12	1D PTFM	Drag+Buoy.	$D_d = \nu_{T,m}/\sigma$	$\nu_{T,d} = \nu_{T,m}$	Standard
13	1D CTFM	Drag+Buoy.	$D_d = \nu_{T,m}$	$\nu_{T,d} = 0$	Standard
14	1D CTFM	Drag+Buoy.	$D_d = \nu_{T,m}$	$\nu_{T,c} = \nu_{T,d}\,(1 + St)$	Standard
15	1D CTFM	Drag+Buoy.	$D_d = D_R$	$\nu_{T,d} = \nu_{T,c}$	Standard
16	1D CTFM	Drag+Buoy.	$D_d = \nu_T + \varepsilon_{drift}$	$\nu_{T,d} = \nu_{T,c}$	Standard

of the disperse phase. We tested: $\nu_{T,d} = 0$ (Run 8) and the relation suggested by Chen and Wood [15], as presented in Eq. 42 (Run 9). In Runs 10–12, we tested diverse versions of the diffusivity of the sediment with the 1D PTFM. We employed the Rousean diffusivity in Run 10; in Run 11, we added the eddy diffusivity of the carrier and the "drift diffusivity" following Czernuszenko. In Run 12, we employed the usual definition, $D_d = \frac{\nu_T}{\sigma}$, in terms of the Schmidt number, σ. In Runs 13–16, we repeated Runs 8–11 with the 1D CTFM instead of the 1D PTFM.

6.3 Discussion of results of mean-flow (time-averaged) variables

Regarding Run 1, it is worth pointing out that if D_d is calculated from the K–ε model instead of using Eq. 15, a close but different curve is obtained. We compare concentration values divided by the concentration C_b, obtained as reported in Sect. 3.6. Figure 3 shows that the computed profiles of velocity and concentration of sediment agree very well with the semi-logarithmic law and with the Rousean distribution, respectively. In other words, Run 1 and the SSTM represent basically Rousean conditions. Results also show that, given the selected spatial step, the numerical scheme does *not* add diffusion artificially to the solution.

6.3.1 Effect of model complexity and coupling

Figures 4–6 show the wall-normal distributions of velocity of the carrier fluid, velocity of the disperse phase and sediment concentrations for Runs 1–3, respectively. The comparisons indicate that the more "sophisticated" 1D PTFM and 1D CTFM do not differ significantly from the 1D SSTM (within 5% from each other) in the prediction of the carrier velocity, and that the 1D PTFM and the 1D CTFM give close values for the velocity of the disperse phase (within 5%). (The 1D SSTM assumes that $U_d = U_m$). Figure 4 also shows that the 1D SSTM and the 1D PTFM give the same velocity profile for the carrier phase. This is expected since

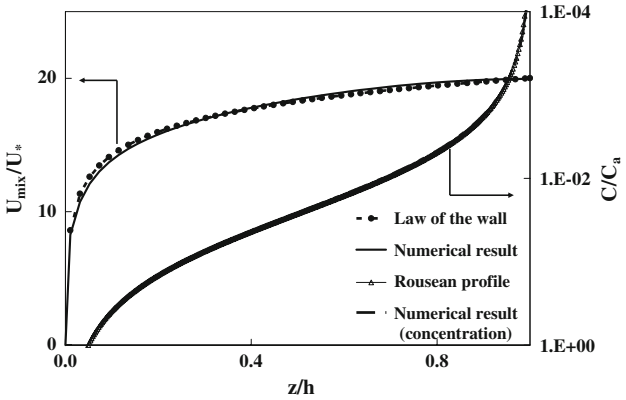

Fig. 3 Comparison of simulated values of the mixture stream-wise velocity and the concentration of sediment obtained from the 1D SSTM with the law of the wall for a rough wall and the Rousean distribution respectively

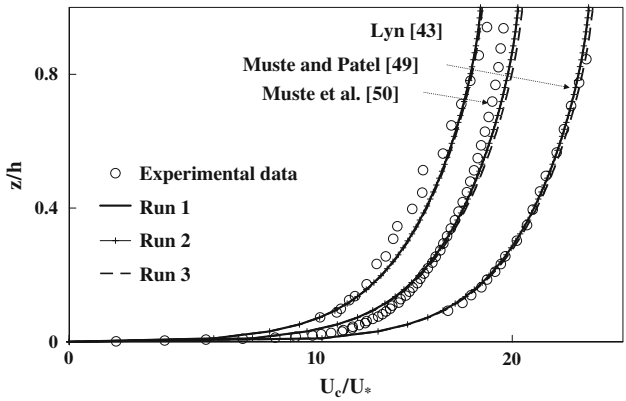

Fig. 4 Comparison of simulated values of the stream-wise velocity for the carrier phase with the experimental data. Simulations were performed using the uncoupled 1D SSTM, the one-way coupled 1D PTFM and the two-way coupled 1D CTFM

the carrier phase is modeled using the same governing equations in both approaches. In general, the models predict the velocities measured by Lyn and Muste and Patel very accurately (within 5%) and the velocities measured by Muste et al. quite accurately (within 10%). In the test corresponding to Muste et al., the models under-predict the velocities (within 10%) for small distances from the wall, and over-predict (within 10%) far from the wall. Table 6 compares the values of the wall-friction (shear) velocity computed with the models and measured by the different authors using diverse methodologies. Clearly, the values are different, as expected, but the differences are within 15%.

However, differences have a significant effect on calculations of the sediment concentrations for the test of Muste et al. (Fig. 6). In this case, the 1D CTFM predicts sediment concentrations which are much smaller than the observed ones, when it should in theory provide closer predictions. These lower values of the sediment concentrations are in line with the larger values of the wall-normal sediment velocity, ($|W_d|$), computed with the CTFM as opposed to the reported (for instance, 0.034 vs. 0.024 m/s for the test by Muste et al.). Interestingly, in the case of Lyn's test (not shown herein), the 1D CTFM and the 1D PTFM

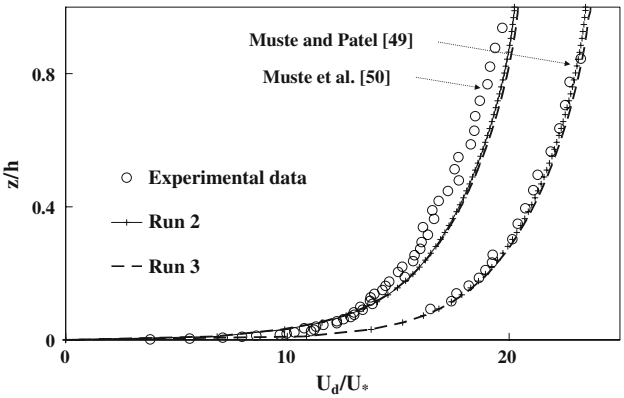

Fig. 5 Comparison of simulated values of the stream-wise velocity for the disperse phase with the experimental data. Simulations were performed using the uncoupled 1D SSTM, the one-way coupled 1D PTFM and the two-way coupled 1D CTFM

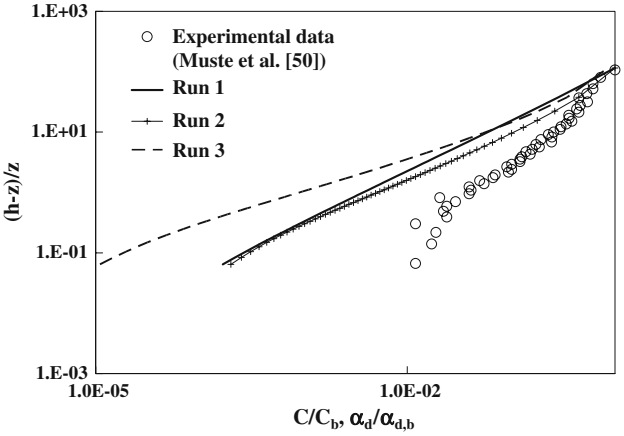

Fig. 6 Comparison of simulated values of the distribution of the concentration of sediment with the experimental data of Muste et al. [50]. Simulations were performed using the 1D SSTM, 1D PTFM and 1D CTFM (Runs 1, 2 and 3, respectively)

provide similar results in terms of sediment concentration, since the predicted wall-normal sediment velocity (0.023 m/s) is almost the same as observed (see Table 4).

Overall, these results suggest that the PTFM offers an improvement over the Rousean profile and that use of the 1D CTFM for dilute sediment transport does not necessarily provide better predictions. Given the number of coefficients involved in the CTFM model, the result can also vary according to the values of those coefficients. This is in agreement with what was shown by Bombardelli et al. [6], and Bombardelli [5] in the context of bubble plumes.

6.3.2 Effect of the interaction forces

In this section, we discuss the effect of adding the lift and virtual mass forces to the drag and buoyancy forces in the momentum equations. From Fig. 7, we note that the results of Runs 2, 4, and 5 overlap in terms of the velocity of the disperse phase, indicating that the

Table 6 Comparison of values of the wall-friction (shear) velocity computed in different ways from the experiments and from our simulations (R: hydraulic radius)

Reference data source	Test case	$U_* = \sqrt{gRS}$	$U_* = \sqrt{ghS}$	U_* reported in the paper	U_* obtained from our code
Lyn [43]	1965EQ	0.0328	0.04	0.0375	0.04
Muste and Patel [49]	SL01	0.0270	0.0307	0.0270, 0.0307	0.03058
Muste et al. [50]	NS01	0.0426	0.0482	0.042	0.04825

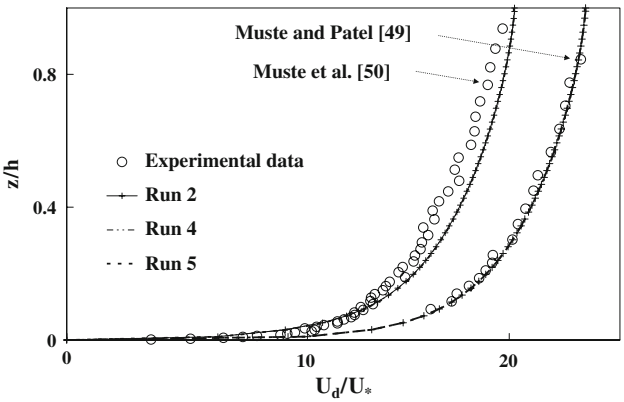

Fig. 7 Comparison of simulated values of the stream-wise velocity for the disperse phase with the experimental data. Simulations were performed using the 1D PTFM together with the interaction forces of drag (Run 2), drag plus lift (Run 4) and drag plus lift and virtual mass (Run 5)

influences of the lift and virtual-mass forces are negligible as compared to the drag force. (This does not mean that they are zero; it means that the forces can be disregarded as opposed to the drag force.) From the numerical results, we divided the lift and virtual mass forces by the drag force and found these ratios to be about 1% for the lift force, and about 2% for the virtual-mass force. Concerning the turbulent-dispersion force [23], we computed the ratio between this force and the drag force. We obtained a value for that ratio below 1% too. This result gives justification to research in which all forces except the drag force have been disregarded, at least for the range of small sand particles moving far from the bed-load layer [8].

Concerning the profiles of sediment concentration and carrier velocity they do not differ significantly from the profiles obtained in Run 2.

6.3.3 Effect of additional terms in the turbulence closure

In Figs. 8 and 9, we compare the predictions of diverse models with data when an extended K–ε closure is employed. Figure 8 shows that the terms proposed by Hsu et al. [31] introduce a slight increase in the velocities of the disperse phase for the data of Muste et al. (within 5%), but that the outcome is almost the same for the data of Muste and Patel: the largest differences in the predicted velocity from Runs 2 and 6 are of the order of 1%. This result is also consistent with the findings of Bombardelli [5], in the context of bubble plumes. Figure 9 corroborates that additional terms in the turbulence closure do not produce major changes even when the 1D CTFM is used, but that differences are even smaller than for the 1D PTFM.

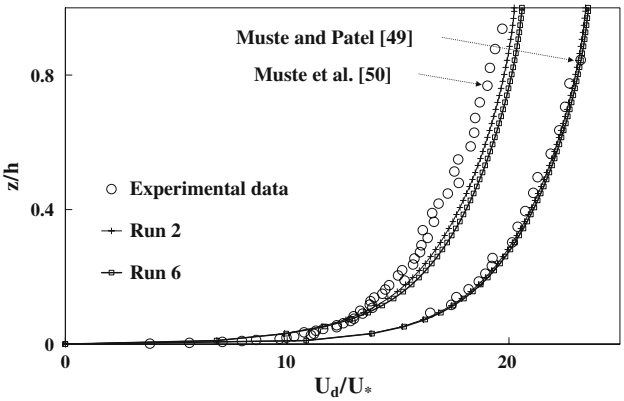

Fig. 8 Comparison of simulated values of the stream-wise velocity for the disperse phase with the experimental data. Simulations were performed employing the 1D PTFM using standard and extended K–ε models (Runs 2 and 6, respectively)

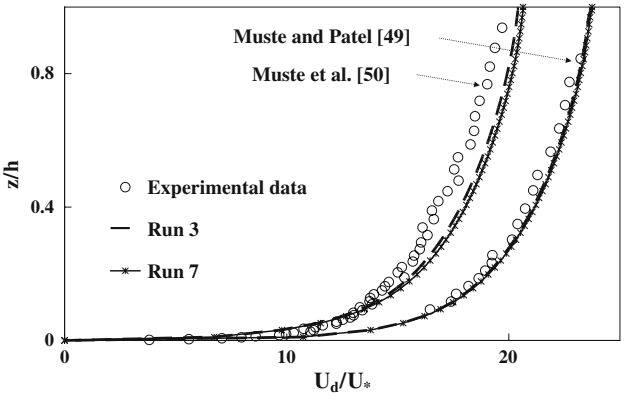

Fig. 9 Comparison of simulated values of the stream-wise velocity of the disperse phase with the experimental data. Simulations were performed using the 1D CTFM together with standard and extended K–ε models (Runs 3 and 7, respectively)

In both cases, similar conclusions can be obtained for the carrier velocity and the sediment concentration, which have almost identical distributions in the wall-normal direction.

6.3.4 Effect of different formulations for the eddy viscosity of the disperse phase ($\nu_{T,d}$)

From Fig. 10, we note that setting the diffusive term to zero in the equations for the x-momentum of the disperse phase (Run 8) produces an improvement of the prediction of the velocity of the disperse phase. This result is in agreement with suggestions by Serizawa et al. [59] (see also [68,69]) for very small ratios of ρ_d/ρ_c, although in this case the density ratio is not small (it is order 1). Figure 10 also shows that the use of the relation of Chen and Wood (Run 9) does not introduce much change in the predictions. The solutions for the velocity of the carrier and the sediment concentration follow similar trends.

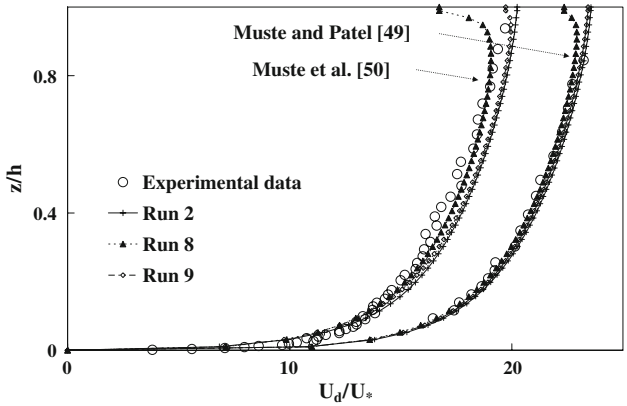

Fig. 10 Comparison of simulated values of the stream-wise velocity of the disperse phase with the experimental data. Simulations were performed employing the 1D PTFM together with different formulations of the eddy viscosity of the disperse phase. The decrease of the velocity of the disperse phase at the top of the water column is an artifact of the use of $\nu_{T,d} = 0$

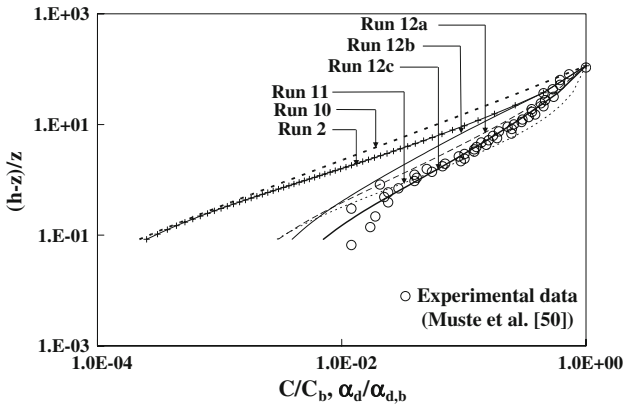

Fig. 11 Comparison of simulated values of the distribution of the concentration of sediment with the experimental data of Muste et al. [50]. Simulations were performed using the 1D PTFM together with different formulations for the sediment diffusion coefficient

6.3.5 Effect of different formulations for the diffusivity of the disperse phase (D_d)

We can observe in Fig. 11 that when the parabolic distribution of Eq. 15 is adopted for the diffusion coefficient (Run 10), the 1D PTFM under-predicts the distribution of sediment concentration throughout the depth (data of Muste et al.). By using the drift described by Czernuszenko [19] (Run 11), the simulated results over-predict near the bottom and under-predict near the top. Similar results were obtained for the data of Lyn (not shown herein).

In Runs 12, we employed different values for the Schmidt number in order to analyze the sensitivity of the numerical solution to this parameter. We computed the Schmidt number from the Van Rijn's [72] formula using the *computed* values of the shear velocity and the settling velocity. We obtained the following values of σ: 0.668 for the selected test by Muste et al., 0.448 for the test by Muste and Patel, and 0.601 for the test by Lyn. With these values, the numerical solution under-predicts in the case of Muste et al.'s data (Run 12a in

Fig. 11), and over-predicts in the case of Lyn's data (not shown). We also employed the variable Schmidt number suggested by Amoudry et al. [1, Eq. 40], which offers σ as a function of the sediment concentration. From the results of Run 12b plotted in Fig. 11, we see that the predictions fall relatively far from the data of Muste et al. Finally, from the results of Run 12c presented in Fig. 11, values of the Schmidt number equal to 0.56 for the dataset of Muste et al., was found to provide the best fit to the data. For the Lyn data, the best fit was found for $\sigma = 0.7$. These values are relatively close to the values computed from the Van Rijn expression, demonstrating the importance of using the proper Schmidt number. It is worth pointing out here that these values of the Schmidt number have been obtained from the developed models, not from the Rousean distribution (cf. [46]). Lyn [46] compiled values for the Schmidt number obtained from the Rousean distribution ranging from 0.3 to more than one, with a large scatter. Our results suggest values of the Schmidt number smaller than one for dilute mixtures.

Using Eq. 41, which relates Czernuszenko's drift formula with the usual definition of the Schmidt number, we obtained average Schmidt numbers (in the depth) of 0.73 for Muste et al.'s, and 0.9 for Lyn's tests. These values are higher than, but nonetheless consistent with, previous values. These numbers explain the differences in predictions using the concept of drift and the measured data.

6.3.6 Test of different boundary conditions

We performed runs using the two-fluid semi-logarithmic velocity law suggested by Troshko and Hassan [68] to address potential changes of the results due to this boundary condition. Our computations showed that the differences between predictions with single- and two-phase boundary conditions were small (see Tables 7 and 8).

6.3.7 Quantitative assessment of the goodness of model predictions

In Table 8, we provide the normalized root mean square error (NRMSE) for several runs. These numbers reflect the same trends signaled before, indicating that there is not much difference between the 1D PTFM and the 1D CTFM.

6.4 Comparison of turbulence statistics

We compared modeled versus measured distributions of the dimensionless TKE in Fig. 12a and modeled versus measured non-dimensional Reynolds shear stresses in Fig. 12b. Measured data is available only for the rms $\sqrt{\overline{u'^2}}$ and $\sqrt{\overline{w'^2}}$ in the datasets of Muste and Patel

Table 7 Comparison of the NRMSE of model runs using boundary conditions as in a single-phase flow (SPFBC) and using the BC proposed by Troshko and Hassan [68] (THBC)

Run	Muste et al. [50]		Muste and Patel [49]	
	$\frac{U_c}{U_*}$	$\frac{U_d}{U_*}$	$\frac{U_c}{U_*}$	$\frac{U_d}{U_*}$
Run 2 using SPFBC	0.057024	0.082868	0.006760	0.010628
Run 2 using THBC	0.054465	0.082347	0.005314	0.014201
Run 3 using SPFBC	0.057321	0.087670	0.006825	0.014848
Run 3 using THBC	0.062177	0.085729	0.007405	0.011402

Table 8 Values of NRMSE for model runs

Runs	Muste et al. [50]		Muste and Patel [49]	
	$\frac{U_c}{U_*}$	$\frac{U_d}{U_*}$	$\frac{U_c}{U_*}$	$\frac{U_d}{U_*}$
Run 2	0.057024	0.082868	0.006760	0.010628
Run 3	0.057321	0.087670	0.006825	0.014848
Run 4	0.057024	0.082299	0.006760	0.010666
Run 5	0.057024	0.080378	0.006760	0.010562
Run 6	0.057223	0.091474	0.005849	0.015527
Run 7	0.057944	0.093183	0.008310	0.018150
Run 8	0.057024	0.075916	0.006760	0.007059
Run 9	0.057024	0.078845	0.006760	0.010124

Normalized root mean square error (NRMSE)= $\sqrt{\frac{1}{N}\sum (Q_{\text{obs}} - Q_{\text{cal}})^2} \Big/ \frac{1}{N}\sum Q_{\text{obs}}$

and Muste et al., where u' and w' indicate the velocity fluctuations in the stream-wise and wall-normal directions, respectively. To be able to compute the TKE, we had to approximate $\sqrt{\overline{v'^2}}$, where v' refers to the span-wise velocity fluctuation. We tested different values for the relation between $\sqrt{\overline{v'^2}}$ and $\sqrt{\overline{u'^2}}$ in order to fit the data, finally obtaining that $\sqrt{\overline{v'^2}} \approx 0.3$–$0.6\sqrt{\overline{u'^2}}$ depending on the dataset. This outcome is different from Nezu and Nakagawa's [52] findings for clear water ($\sqrt{\overline{v'^2}} = 0.71\sqrt{\overline{u'^2}}$). More experimental data is needed to address this difference in detail.

In Fig. 12a, we show that both the 1D PTFM and the 1D CTFM predict closely the measured distributions of TKE for dimensionless wall-normal distances up to 0.65 in the tests of Muste and Patel. Again, the 1D CTFM performs no better than the 1D PTFM, and the addition of the terms introduced by Hsu et al. [31] does not provide much difference either. A similar behavior of the numerical results was observed for the dataset of Muste et al.

The agreement is not satisfactory close to the free surface. Small undulations at the air–water interface (i.e., departures from an absolutely flat surface) might be responsible for generating turbulence in the free-surface boundary layer. Note that the data indicates that $K \neq 0$ at the free surface. We tested other BCs and found that the use of $\frac{\partial K}{\partial z} = 0$ as boundary condition therein does not provide better agreement with the data (not shown).

In Fig. 12b, we note that our numerical results follow quite closely the observations by Muste and Patel and Muste et al. regarding the Reynolds shear stresses. It is well known that in the case of clear-water flow, the Reynolds shear stresses follow a straight line. Graf and Cellino [27] and Best et al. [3] observed in their experiments no considerable departure of the Reynolds stresses in sediment-laden flows from their clear-water counterparts. Our runs with both the 1D PTFM and the 1D CTFM follow the observations very well.

7 Final remarks and conclusions

We have developed a rigorous hierarchy of models for *dilute*, sediment-laden, open-channel flows, using an Eulerian–Eulerian approach. Although some similar models have been used in the past in different versions and formats, this is the first time, to the best of our knowledge, that a framework deriving each component as a special case of more general equations is presented. Further, this is the first time that different models are consistently tested against three recent datasets. We consider this framework to be very useful in providing different

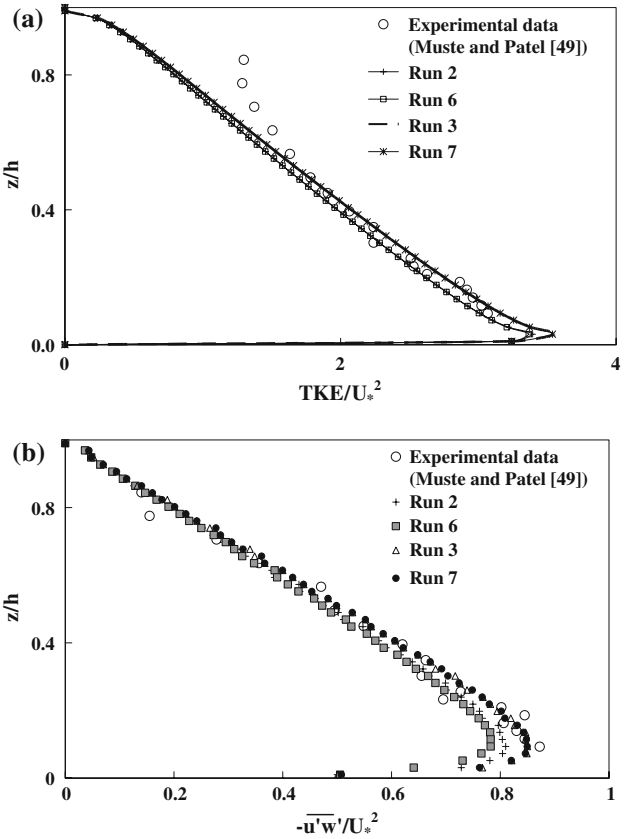

Fig. 12 (**a**) Comparison of simulated values of the turbulent kinetic energy of the carrier phase with the experimental data of Muste and Patel [49]. Simulations were performed using the 1D PTFM and 1D CTFM together with standard and extended K–ε models (Runs 2, 3, 6, 7, respectively). (**b**) Comparison of simulated values of the Reynolds shear stress for the carrier phase with the experimental data of Muste and Patel [49]. Simulations were performed using the 1D PTFM together with standard and extended K–ε models (Run 2, 3, 6, and 7, respectively)

alternatives for the prediction of sediment transport. Within that framework, we investigated several issues related especially to model complexity, turbulence closures, and turbulent diffusivities. Very importantly, we compared for the first time predicted and modeled two-phase *turbulence statistics in sediment transport*.

Our numerical computations show that most models analyzed in this paper predict relatively accurately the velocity field (within 5–10%). However, only a few of those models predict accurately the concentration of sediment and the turbulence statistics. We showed that the PTFM (which introduces two-phase equations for the disperse phase but keeps mixture variables for the water) already brings a substantial improvement with respect to the Rousean distribution. We also showed that although the 1D CTFM should in principle be more accurate given its greater complexity and "rigor," it does not provide significant improvement over the more simple 1D PTFM in dilute mixtures.

We found that the forces of lift and virtual mass are small in comparison to the drag force, and that for the presented data the former can be disregarded. Although this is a well-known

result for particles moving in *gas* streams (see [62]) our results extend this notion to sand particles moving in water (about 100–200 microns in diameter).

The predicted turbulent statistics from the developed models are not close to the measured datasets near the free surface, but they are very close to the data up to 0.65 and close up to 0.75. Additional terms that have been recommended for the $K-\varepsilon$ model in two-phase flows do not lead to much difference in the prediction of flow variables. Thus, the *standard* $K-\varepsilon$ model appears to be suitable to the simulation of boundary-layer problems in two-phase flows, at least for dilute mixtures; this result is in agreement with computations of bubble plumes (see [4–6,10]).

Our simulations allowed us to obtain values of the Schmidt number that fit the datasets from the models, not from the Rousean profile. These values are 0.7 and 0.56 for the tests of Lyn, and Muste et al., respectively, which agree reasonably well with the values obtained from the Van Rijn equation: 0.601 and 0.668 for such datasets, respectively. All these values are smaller than 1, indicating that the diffusivity of momentum of the carrier fluid (the eddy viscosity) is smaller than the diffusivity of sediment. This result is in agreement with the vast majority of the literature [50,51,72] and it agrees very well with values used for bubble plumes (of the order of 0.83; see [5]). Through comparison with data, results of the numerical models predict that the ratio between the rms in the span-wise and stream-wise directions was about 0.3–0.6 in those tests.

Acknowledgements This paper was completed thanks to funding awarded by the University of California Water Resources Center (UC WRC) to Profs. Stefan Wuertz and Fabián A. Bombardelli. Comments by Dr. M. Muste and Prof. G. C. Buscaglia are also gratefully acknowledged.

References

1. Amoudry L, Hsu TJ, Liu PL (2005) Schmidt number and near-bed boundary condition effect on a two-phase dilute sediment transport. J Geophys Res 110(C09003). doi:10.1029/2004JC002798
2. Axell L (2002) Wind-driven internal waves and Langmuir circulations in a numerical ocean model of the southern Baltic Sea. J Geophys Res. doi:10.1029/2001JC000922
3. Best J, Bennett S, Bridge J, Leeder M (1997) Turbulence modulation and particle velocities over flat sand beds at low transport rates. J Hydrol Eng 123(12):1118–1128. doi:10.1061/(ASCE)0733-9429(1997)123:12(1118)
4. Bombardelli FA (2003) Characterization of coherent structures from parallel, LES computations of wandering effects in bubble plumes. In: Proceedings of the 2003 world water & environmental resources congress, June 2003, Philadelphia, PA, EWRI/ASCE
5. Bombardelli FA (2004) Turbulence in multiphase models for aeration bubble plumes. PhD Thesis, Department of Civil and Environmental Engineering, University of Illinois at Urbana-Champaign
6. Bombardelli FA, Buscaglia GC, García MH (2003) Parallel computations of the dynamic behavior of bubble plumes. In: Brust FW (ed) Proceedings of the pressure vessels and pipe division conference. Cleveland, vol PVP-464, Residual Stress, Fitness-for-Service, and Manufacturing Processes. ASME-PVP Division
7. Bombardelli FA, Buscaglia GC, Rehmann CR, Rincon LE, García MH (2007) Modeling and scaling of aeration bubble plumes: a two-phase flow analysis. J Hydraul Res 45(5):617–630
8. Bombardelli FA, González AE, Niño YI (2008) Computation of the Basset force with a fractional-mathematics approach. J Hydr Eng, ASCE (in Press)
9. Brennen E (2005) Fundamentals of multiphase flow. Cambridge Press, New York
10. Buscaglia GC, Bombardelli FA, García MH (2002) Numerical modeling of large scale bubble plumes accounting for mass transfer effects. Int J Multiph Flow 28:1763–1785. doi:10.1016/S0301-9322(02)00075-7
11. Cao Z, Wei L, Xie J (1995) Sediment-laden flow in open channels from two-phase flow viewpoint. J Hydrol Eng 121(10):725–735. doi:10.1061/(ASCE)0733-9429(1995)121:10(725)

12. Carrica P, Bonetto F, Drew D, Lahey R (1998) The interaction of background ocean air bubbles with a surface ship. Int J Numer Methods Fluids 28:571–600. doi:10.1002/(SICI)1097-0363(19980930)28:4<571::AID-FLD731>3.0.CO;2-E
13. Carrica P, Drew D, Bonetto F, Lahey R (1999) A polydisperse model for bubbly two-phase flow around a surface ship. Int J Multiph Flow 25:257–305. doi:10.1016/S0301-9322(98)00047-0
14. Cellino M, Graf WH (2002) Suspension flow in open channels; experimental study. J Hydraul Res 15:435–447
15. Chen CP, Wood PE (1986) Turbulence closure modeling of the dilute gas-particle axisymmetric jet. AIChE J 32(1):163–166. doi:10.1002/aic.690320121
16. Chien N, Wan Z (1999) Mechanics of sediment transport. ASCE Press, USA
17. Coleman NL (1986) Effects of suspended sediment on the open-channel distribution. Water Resour Res 22(10):1377–1384. doi:10.1029/WR022i010p01377
18. Crowe CT, Sommerfeld M, Tsuji Y (1998) Multiphase flows with droplets and particles. CRC Press, Florida
19. Czernuszenko W (1998) Drift velocity concept for sediment-laden flows. J Hydrol Eng 124(10):1026–1033. doi:10.1061/(ASCE)0733-9429(1998)124:10(1026)
20. Dietrich WE (1982) Settling velocity of natural particles. Water Resour Res 18(6):1626–1632. doi:10.1029/WR018i006p01615
21. Dong P, Zhang K (1999) Two-phase flow modeling of sediment motions in oscillatory sheet flow. Coast Eng 36:87–109. doi:10.1016/S0378-3839(98)00052-0
22. Drew DA (1975) Turbulent sediment transport over a flat bottom using momentum balance. J Appl Mech 42:38–44
23. Drew D, Passman S (1999) Theory of multicomponent fluids. Applied mathematical sciences, vol 135. Springer, New York
24. Einstein HA, Chien N (1955) Effects of heavy sediment concentration near the bed on velocity and sediment distribution. MRD Sediment Ser Rep No 8. Univ of California, Berkeley, US Army Corps of Engineers, Missouri Div
25. Elghobashi SE, Abou-Arab TW (1983) A two-equation turbulence model for two-phase flows. Phys Fluids 26(4):931–938. doi:10.1063/1.864243
26. Ferziger JH, Peric M (2002) Computational methods for fluid dynamics. Springer, New York
27. Graf WH, Cellino M (2002) Suspension flows in open channels: experimental study. J Hydraul Res 40(4):435–447
28. Greimann BP, Muste M, Holly FM Jr (1999) Two-phase formulation of suspended sediment transport. J Hydraul Res 37:479–500
29. Greimann BP, Holly FM Jr (2001) Two-phase flow analysis of concentration profiles. J Hydrol Eng 127(9):753–762. doi:10.1061/(ASCE)0733-9429(2001)127:9(753)
30. Guo J, Julien PY (2001) Turbulent velocity profiles in sediment-laden flows. J Hydraul Res 39(1):11–23
31. Hsu T, Jenkins JT, Liu PLF (2003a) On two-phase sediment transport: dilute flow. J Geophys Res 108(C3):3057. doi:10.1029/2001JC001276
32. Hsu T, Chang H, Hsieh C (2003b) A two-phase flow model of wave-induced sheet flow. J Hydraul Res 41(3):299–310
33. Jiang J, Law AW, Cheng N-S (2004) Two-phase analysis of vertical sediment laden jets. J Eng Mech 131(3):308–318. doi:10.1061/(ASCE)0733-9399(2005)131:3(308)
34. Kataoka I, Serizawa A (1989) Basic equations of turbulence in gas-liquid two-phase flow. Int J Multiph Flow 15(5):843–855. doi:10.1016/0301-9322(89)90045-1
35. Kobayashi N, Seo SN (1985) Fluid and sediment interaction over a plane bed. J Hydrol Eng 111(6):903–919
36. Lain S, Aliod R (2000) Study on the Eulerian dispersed phase equations in non-uniform turbulent two-phase flows: discussion and comparison with experiments. Int J Heat Fluid Flow 21:374–380. doi:10.1016/S0142-727X(00)00023-0
37. Landau L, Lifshitz E (2000) Fluid mechanics. Pergamon, Oxford
38. Launder BE, Spalding DB (1973) The numerical computation of turbulent flows. Comput Methods Appl Mech Eng 3:269–289. doi:10.1016/0045-7825(74)90029-2
39. Liu H, Sato S (2006) A two-phase flow model for asymmetric sheetflow conditions. Coast Eng 53:825–843. doi:10.1016/j.coastaleng.2006.04.002
40. Longo S (2005) Two-phase flow modeling of sediment motion in sheet-flows above plane beds. J Hydrol Eng 131(5):366–379. doi:10.1061/(ASCE)0733-9429(2005)131:5(366)
41. Loth E (2007) Computational fluid dynamics of bubbles, drops and particles. Cambridge University Press, Cambridge

42. Lyn DA (1986) Turbulence and turbulent transport in sediment-laden open channel flows. PhD Thesis, Calif Inst of Technol, Pasadena
43. Lyn DA (1988) A similarity approach to turbulent sediment-laden flows in open channels. J Fluid Mech 193:1–26. doi:10.1017/S0022112088002034
44. Lyn DA (1991) Resistance in flat-bed sediment-laden flows. J Hydrol Eng 117(1):94–114. doi:10.1061/(ASCE)0733-9429(1991)117:1(94)
45. Lyn DA (1992) Turbulence characteristics of sediment-laden flows in open channels. J Hydrol Eng 118(7):971–987. doi:10.1061/(ASCE)0733-9429(1992)118:7(971)
46. Lyn DA (2008) Sedimentation engineering: theories, measurements, modeling and practice. In: García M (ed) Manual No 110, ASCE
47. McTigue DF (1981) Mixture theory for suspended sediment transport. J Hydraul Div 107(HY6): 659–673
48. Moraga FJ, Larreteguy AE, Drew DA, Lahey RT (2003) Assessment of turbulent dispersion models for bubbly flows in the low Stokes number limit. Int J Multiph Flow 29(4):655–673. doi:10.1016/S0301-9322(03)00018-1
49. Muste M, Patel VC (1997) Velocity profiles for particles and liquid in open-channel flow with suspended sediment. J Hydrol Eng 123(9):742–751. doi:10.1061/(ASCE)0733-9429(1997)123:9(742)
50. Muste M, Fujita K, Yu I, Ettema R (2005) Two-phase versus mixed-flow perspective on suspended sediment transport in turbulent channel flows. Water Resour Res 41:W10402. doi:10.1029/2004WR003595
51. Nezu I, Azuma R (2004) Turbulence characteristics and interaction between particles and fluid in particle-laden open channel flows. J Hydrol Eng 130:988–1001. doi:10.1061/(ASCE)0733-9429(2004)130:10(988)
52. Nezu I, Nakagawa H (1993) Turbulence in open-channel flow. IAHR Monograph. A A Balkema Publishers, Rotterdam
53. Nezu I, Rodi W (1986) Open-channel flow measurements with a laser doppler anemometer. J Hydrol Eng 112:335–355
54. Parker G (2004) 1D sediment transport morphodynamics with application to rivers and turbidity currents. e-book downloadable at: http://cee.uiuc.edu/people/parkerg/morphodynamics_ebook.htm
55. Patankar SV (1980) Numerical heat transfer and fluid flow. Hemisphere, New York
56. Prosperetti A, Zhang DZ (1995) Finite-particle-size effects in disperse two-phase flows. Theor Comput Fluid Dyn 7:429–440. doi:10.1007/BF00418141
57. Rodi W (1984) Turbulence models and their application in hydraulics. International Association for Hydraulic Research, Delft, The Netherlands
58. Rouse H (1937) Modern conception of the mechanics of turbulence. Trans ASCE 102:463–543
59. Serizawa A, Kataoka I, Michiyosi I (1975) Turbulence structure of air-water flows: parts 1–3. Int J Multiph Flow 21(3):221–259. doi:10.1016/0301-9322(75)90011-7
60. Sokolichin A, Eigenberger G (1999) Applicability of the standard turbulence model to the dynamic simulation of bubble columns: part I. Detailed numerical simulations. Chem Eng Sci 54:2273–2284. doi:10.1016/S0009-2509(98)00420-5
61. Sokolichin A, Eigenberger G, Lapin A (2004) Simulation of buoyancy driven bubbly flow: established simplifications and open questions. AIChE J 50:24–45. doi:10.1002/aic.10003
62. Sommerfeld M (1992) Modelling of particle-wall collisions in confined gas-particle flows. Int J Multiph Flow 18:905–926. doi:10.1016/0301-9322(92)90067-Q
63. Svensson U (1998) Program for boundary layers in the environment—system description and manual. SMHI Reports. Oceanography 24:42 pp
64. Svensson U, Sahlberg J (1989) Formulae for pressure gradients in one-dimensional lake models. J Geophys Res 94:4939–4946. doi:10.1029/JC094iC04p04939
65. Svensson U, Axell L, Sahlberg J, Omstedt A (2002) Program for boundary layers in the environment—system description and manual
66. Taggart WC, Yermoli CA, Montes S, Ippen AT (1972) Effects of sediment size and gradation on concentration profiles for turbulent flow. MIT Report No 152
67. Tomiyama A, Shimada N (2001) A numerical method for bubbly flow simulation based on a multi-fluid model. Trans ASME J Press Vessel Technol 123(4):510–520. doi:10.1115/1.1388010
68. Troshko AA, Hassan YA (2001a) A two-equation turbulence model of turbulent bubbly flows. Int J Multiph Flow 27:1965–2000. doi:10.1016/S0301-9322(01)00043-X
69. Troshko AA, Hassan YA (2001b) Law of the wall for two-phase turbulent boundary layers. Int J Heat Mass Transfer 44:871–875. doi:10.1016/S0017-9310(00)00128-9
70. Vanoni VA (1946) Transportation of suspended sediment by water. Trans ASCE 111:67–133
71. Vanoni VA (1975) Suspension of sediment. In: Vanoni VA (ed) Sedimentation engineering. ASCE, New York

72. Van Rijn LC (1984) Sediment transport. Part II: suspended load transport. J Hydrol Eng 110(11): 1613–1641
73. Villaret C, Davies AG (1995) Modeling sediment-turbulent flow interactions. Appl Mech Rev 48(9):601–609
74. Wang X, Qian N (1992) Velocity profiles of sediment laden flow. Int J Sediment Res 7(1):27–58
75. Zhang D, Deen NG, Kuipers JAM (2006) Numerical simulation of the dynamic flow behavior in a bubble column: a study of closures for turbulence and interface forces. Chem Eng Sci 61:7593–7608. doi:10.1016/j.ces.2006.08.053